Journal of Materials Chemistry A

Accepted Manuscript

ROYAL SOCIETY OF CHEMISTRY

www.rsc.org/materialsA

Alkali metals incorporated ordered mesoporous tantalum oxide with enhanced photocatalytic activity for water splitting

Tobias Grewe, and Harun Tüysüz*

Max-Planck-Institut für Kohlenforschung, Kaiser-Wilhelm-Platz 1, 45470 Mülheim an der Ruhr, Germany

tueysuez@kofo.mpg.de

Abstract

Herein, we report a novel synthetic approach for the preparation of alkali (Na, K) metal incorporated ordered mesoporous tantalate composites and their photocatalytic performance for water splitting. With the main focus on sodium based composite materials, a series of samples with ordered mesoporosity and high surface area (108-120 m^2 g^{-1}) was prepared by a variation of the Ta/Na ratios through a soft templating route. The structural parameters and properties of the samples were analyzed by low angle XRD, N_2-physisorption, TEM and STEM analysis, EDX, XPS, Raman and diffuse reflectance UV-Vis spectroscopy. The incorporation of alkali metals resulted in ordered mesoporous tantalate composites. Furthermore, the addition of alkaline earth (Ca, Ba, Sr) metals to the precursor solution of ordered mesoporous tantalum oxide was attempted. However, alkaline earth metals gave unordered tantalate composites. Photocatalytic investigations for water splitting, by using methanol as a sacrificial agent, indicated that the incorporation of alkali metals enhanced the hydrogen production rate of the photocatalyst whereas addition of alkaline earth metals decreased the hydrogen production. Among the sodium based samples, a Ta/Na ratio of 9 showed the best performance. The efficiency of this sample was further improved through decorated NiO_x as co-catalyst. A 2.5 wt-% NiO_x loading was found to be the optimal loading amount, generating 64 µmol h^{-1} H_2 and 31 µmol h^{-1} O_2 when tested for overall water splitting.

Introduction

Amongst renewable energy sources, solar energy has gained considerable attention as the sun can supply about four orders of magnitude (10^4 times) higher energy to the earth's surface than global energy consumption.[1] In an attempt to generate new energy carriers, the production of hydrogen as solar fuel is widely investigated since it can be stored, transported, converted into more convenient fuels like methane, and can release its energy on demand in a fuel cell process.[2] Hydrogen can be produced through photocatalytic water splitting by converting the solar energy directly into chemical energy. For this process, the design of photocatalysts and engineering of the crucial parameters such as band gap, surface structure, morphology, catalyst/solution, and catalyst/co-catalyst interfaces is an emerging field in the development of suitable semiconductors.[3] In particular, progress is driven towards nanostructured materials as they offer benefits for solar water splitting that increase solar-to-hydrogen conversion efficiency.[4-6]

Nanostructured materials show different physical and chemical properties than bulk materials which are beneficial for photocatalytic water splitting such as a high surface area, offering a large number of catalytic sites and short carrier diffusion paths to the surface of the catalyst. These short diffusion paths decrease the probability of charge carrier recombination and thus increase the overall efficiency of the semiconductor.[6, 7, 8] Furthermore, an effective charge separation, which can be achieved through the formation of heterojunctions or composite materials, enhances the activity of the photocatalyst.[9, 10, 11] These unique physical and chemical features are the driving force for the investigation of a broad range of nanomaterials for photocatalytic hydrogen production.[4, 8, 12] Among semiconductor materials**,** tantalates have received much attention due to their high efficiency and as a model system for photocatalytic applications. Perovskite tantalate photocatalysts with the chemical formula of $ATaO_3$ with A = Li, Na, K and pyrochlore $BaTa_2O_6$ were first reported as water splitting catalysts by Kato and Kudo.[13] In the following years, $ATaO_3$ (A = Li, Na, K) was investigated in more depth as a photocatalyst for overall water splitting together with alkaline earth tantalates $A'Ta_2O_6$ (A' = Ca, Ba, Sr).[14, 15] A detailed overview of tantalum-based semiconductors for solar water splitting can be found in recent review articles.[16, 17]

A wide range of preparation methods for nanostructured photocatalysts is known mostly based on top-down and bottom-up approaches.[18] To prepare materials with a well-defined

nanostructured morphology, common methods such as soft templating,[19, 20] hard templating,[21] hydrothermal synthesis,[11, 22] and electrophoretic deposition[23] or anodization[24] are often used. In case of templating methods, nanostructured semiconductor materials with tunable dimension, morphology, geometry and symmetry, and textural parameters can be prepared, showing an advantage over other synthetic procedures. Particularly, soft templating offers a scalable synthesis method for preparation of ordered mesoporous materials (OMMs). This class of materials offers many advantages such as well-defined structure, long range ordered array and narrow pore size distribution, high surface area, and large pore volume. In addition, they provide an outstanding platform (pore confinement) for the deposition of other active components for various catalytic applications.[25]

A general soft-templating procedure was reported for the preparation of various ordered mesoporous materials by Stucky and co-workers.[26] In this procedure, the metal precursors, which were metal chlorides, were dissolved in an alcohol solution containing a poly(alkylene oxide) block copolymer. The metal chlorides react with the alcohol and form a sol solution. Subsequently, the sol solutions were dried and calcined, yielding mostly hexagonal ordered mesoporous metal oxides. Of the metal oxides, also mesoporous Ta_2O_5 was synthesized. However, the ordering of this material was not as good as of other metal oxides prepared by that procedure. In order to obtain a Ta_2O_5 with a highly ordered mesoporous structure, the synthesis protocol was further improved.[27] By adjusting the amount of tantalum chloride in the alcohol/block copolymer solution and optimizing the amount of water (which hydrolysis the tantalum precursor), a highly ordered mesoporous tantalum oxide with a hexagonal symmetry was obtained.

Catalysts obtained via soft templating are commonly amorphous; however, by post-treatment methods these materials can be crystallized.[28] In photocatalysis it is accepted that crystallinity is a key requirement for high catalytic activity.[16] The ordered atomic structure allows charge carriers to diffuse faster than in an amorphous structure, in which charge carrier recombination occurs with a higher probability due to the high defect density of the amorphous structure.[29] It was shown, however, that a partially crystalline structure that consists of different phases can have a higher photocatalytic activity than its pure crystalline counterpart.[10] Furthermore, a few results were presented where amorphous material shows higher activity for solar water splitting than crystalline equivalents.[30, 31] Amorphous materials have benefits in terms

of high surface area, nanostructured surface and less bulk material, e.g. small particles or thin walls of porous material, which favor the migration of excited electrons to the surface. In addition, this type of material usually needs a lower preparation temperature than their crystalline counterparts, making it more favorable for large scale application.[32]

As a photocatalyst, tantalum oxide shows almost no activity for overall water splitting, but overall water splitting was achieved through the decoration of a co-catalyst.[33, 34] Conversely, sodium tantalates and mixtures of tantalates were very active photocatalysts, also for overall water splitting.[10, 11, 15, 35] Therefore, new synthesis routes of ordered mesoporous sodium loaded tantalum oxides are essential for development of more effective photocatalysts.

Herein, we present a novel synthetic method to prepare various amorphous composite materials by adding alkali and alkaline earth metals into the structure of mesoporous tantalum oxide. The main emphasis was given to the incorporation of Na, since among the alkali metal tantalates Na-based tantalates have been shown to have the best performance for water splitting.[15] The incorporation of alkali metals (Na and K) keeps the ordered mesoporous structure intact while the addition of alkaline earth metals (Ca, Ba, Sr) result in unordered composites. Na and K based composite materials showed superior performance for water splitting in comparison to ordered mesoporous Ta_2O_5. The highest H_2 production rate was observed for sodium incorporated ordered mesoporous tantalum oxide with Ta/Na ratio of 9 and 2.5 wt-% NiO_x as co-catalyst.

Experimental

Sodium hydroxide (NaOH), and potassium hydroxide (KOH) were purchased from VWR. Tantalum(V) ethoxide ($Ta(OEt)_5$, 99.98 % trace metals basis), tantalum(V) chloride ($TaCl_5$, 99.8 % trace metals basis), tantalum(V) oxide (Ta_2O_5< 5 micron, 99.99 %), sodium ethoxide (Na(OEt), technical grade ≥ 95 %), nickel nitrate hexahydrate ($Ni(NO_3)_2 \cdot 6H_2O$, purum p.a. ≥ 97 %), calcium hydroxide ($Ca(OH)_2$, puriss p.a. ≥ 96 %), barium hydroxide octahydrate ($Ba(OH)_2 \cdot 8H_2O$, puriss p.a. ≥ 98 %), strontium hydroxide octahydrate ($Sr(OH)_2 \cdot 8H_2O$, 95 %), and Pluronic P123 were obtained from Sigma Aldrich. Na_2CO_3 (99.8 %) was purchased from Acros Organics. All chemicals were used as-received without further purification. Ethanol was

dried using a 3 Å molecular sieve (Merck). $Ba(OH)_2 \cdot 8H_2O$ and $Sr(OH)_2 \cdot 8H_2O$ were dried before usage at 100 °C overnight.

Preparation of ordered mesoporous tantalum oxide (om-Ta_2O_5): Ordered mesoporous tantalum oxide was prepared via soft-templating based on a reported synthesis.[27] Pluronic P123 (4.512 g) was dissolved in 22.7 mL dry ethanol (*dried via molecular sieve*) under vigorous stirring. A second solution was prepared by adding $TaCl_5$ (9.69 g) to 22.7 mL dry ethanol. After dissolving, both solutions were mixed together and a small amount of water (0.488 mL) was added to start the hydrolysis. The final mixture was stirred for 1 h before it was homogeneously distributed over five glass Petri dishes (diameter ~ 12 cm). The dishes were placed in an oven at 40 °C for 1 week. To recover the sample, the dried films were scraped off from the dishes and finely grounded. At last, Pluronic P123 was removed by calcination at 550 °C for 10 h (ramping: 5 °C min^{-1}).

Preparation of ordered mesoporous sodium loaded tantalum oxide (om-TaNa): For the ordered mesoporous sodium loaded tantalum oxide samples $Ta(OEt)_5$ was used as precursor and sodium hydroxide was added as Na^+ and OH^- source. In a typical reaction, 0.5 g Pluronic P123 was dissolved in 5 mL dry ethanol and 1.56 mL $Ta(OEt)_5$ was added to solution. Different amounts of sodium hydroxide (0.286, 0.67, 1.2, 2 mmol) were dissolved in another mixture of 0.5 g Pluronic P123 and 5 mL of dry ethanol. While stirring, the sodium hydroxide solution was slowly added to the $Ta(OEt)_5$ solution. 0.098 mL water was added and the final mixture was stirred for another hour. Afterwards, the solution was poured into a Petri dish (diameter: 12 cm) and dried at 40 °C for 1 week. The dry material was collected, grounded and calcined at 550 °C for 4 h (ramping: 5 °C min^{-1}).

Preparation of om-TaX with a Ta / X ratio of 9 (X = K, Ca, Ba, Sr): In this synthesis, the tantalum precursor solution was prepared as described before. It was mixed with a solution consisting of 5 mL ethanol, 0.5 g Pluronic P123 and 0.67 mmol alkali or alkaline earth metal hydroxide (KOH, $Ca(OH)_2$, $Ba(OH)_2 \cdot 8H_2O$, or $Sr(OH)_2 \cdot 8H_2O$). After adding 0.098 mL of water, the mixture was stirred for 1 h and subsequently transferred into a Perti dish (diameter: 12 cm) and dried at 40 °C for 1 week. The final product was grounded and calcined at 550 °C for 4 h (ramping: 5°C min^{-1}).

Co-catalyst loading: 100 mg of catalyst was decorated with various loadings of NiO_x (0.5, 1, 2.5 and 5 wt-%) as a co-catalyst. In a typical reaction (2.5 wt-% loading), 9.7 mg $Ni(NO_3)_2 \cdot 6H_2O$ was dissolved in 2 mL ethanol and subsequently 100 mg of catalyst was added to the solution and stirred for 1 h. The solvent was evaporated at 50 °C overnight. The dried sample was calcined in H_2 flow (200 mL min^{-1}) at 400 °C for 2 h and then in air at 200 °C for 1 h (ramping: 5 °C min^{-1}).

Preparation of SS-$NaTaO_3$ as reference for Raman spectroscopy. $NaTaO_3$ was prepared via solid-solid state synthesis[11, 36] and is designated SS-$NaTaO_3$. A solid mixture of Ta_2O_5 (0.442 g) and Na_2CO_3 (0.113 g, 5% excess) was thoroughly ground and afterwards calcined at 900 °C for 1 h (with a ramping rate of 5 °C/min), then cooled down to room temperature and ground again. Subsequently, the material was calcined at 1150 °C for 10 h with a ramping of 5 °C/min. Finally, excess sodium was washed out with water.

Characterization: Transmission electron microscopy (TEM) images were obtained with an H-7100 electron microscope (100 kV acceleration voltage) from Hitachi. High resolution transmission electron microscopy (HR-TEM) images were obtained with an HF-2000 microscope (Hitachi) equipped with a cold field emission gun. The acceleration voltage was 200 kV. Samples were prepared on carbon film covered grids. STEM images and elemental mapping were performed on a Hitachi HD-2700 C_S-corrected Scanning Transmission Electron Microscope (STEM) operated at 200 kV equipped with an EDAX Octane T Ultra W EDX detector. Nitrogen physisorption isotherms of samples were measured with an ASAP 2010 analyser (Micrometrics) at 77 K. Prior to the measurements, the samples were degassed at 120 °C for 12 h. Total pore volumes were determined using the adsorbed volume at 0.97 p/p_0. BET (Brunauer-Emmett-Teller) surface area was determined from the relative pressure range between 0.06 and 0.2. XRD patterns were collected at room temperature on a Stoe theta/theta diffractometer in Bragg-Brentano geometry (Cu $K\alpha_{1/2}$ radiation). The measured patterns were evaluated qualitatively by comparison with entries from the ICDD-PDF-2 powder pattern database. EDX spectroscopy was conducted on a Hitachi S-3500N. The microscope is equipped with a Si(Li) Pentafet Plus-Detector from Texas Instruments. Ultraviolet and visible light spectroscopy (UV-VIS) was conducted in diffuse reflectance mode on a Varian Cary 5G with praying mantis set-up using MgO as white standard. Tauc plots were derived from UV-Vis spectra via the Kubelka-Munk

function, treating the materials as indirect semiconductors. Raman spectroscopy was conducted using the QE65 Pro from Ocean Optics with an excitation wavelength of 785 nm using a Turnkey Raman Laser. The powder samples were prepared with a flat surface on a glass holder as analyzed from 1 cm distance by the Raman probe.

Photocatalytic H_2 production: Photocatalytic H_2 production was conducted with an in-house built inner irradiation photoreactor cell with a total volume of 260 mL. For water splitting with a sacrificial agent, the reactor was filled with 200 mL of a water/methanol solution (10 vol-% methanol in deionized water). Overall water splitting was performed with 200 mL of deionized water. 100 mg of solid catalyst was dispersed in 10 mL reactor solution and sonicated for 20 min before it was mixed with the rest of the solution and poured into the reactor. To ensure a good mixing, the solution inside the photoreactor was stirred during the catalytic test. A 150 W middle pressure mercury lamp (TQ 150) from Peschl Ultraviolet was used as a light source. A typical reaction time was 2 h for hydrogen production from water/methanol mixture. An Ar flow of 50 mL min^{-1} was connected to the reactor and purged through the solution, carrying the evolved gases out of the reactor via another connection into a gas analyser (X-STREAM Enhanced XEGP Gas Analyzer from Emerson) equipped with a detector for carbon dioxide (infrared detector), oxygen (paramagnetic detector) and hydrogen (heat conductivity detector). For overall water splitting measurements the samples were irradiated until hydrogen and oxygen were generated in stoichiometric ratio, then the light was switched off and the reactor set-up was purged with argon to remove all traces of hydrogen and oxygen. Subsequently, the lamp was switched on and hydrogen and oxygen evolution rates were measured.

Results and Discussion

Ordered mesoporous materials possess typical long range ordered arrangement and narrow pore size distribution that can be identified with low angle X-ray diffraction (XRD) and microscopic investigations. Ordered mesoporous tantalum oxide (om-Ta_2O_5) and sodium loaded tantalum oxide samples (om-TaNa) were prepared via soft templating and after template removal the materials were characterized by low angle XRD and transmission electron microscopy (TEM). As seen in **Figure 1a**, the low angle XRD pattern of om-Ta_2O_5 shows a strong reflex around 1.5° 2θ and an additional broad reflex at 2.5° 2θ, which is in good agreement with previously reported om-Ta_2O_5.[26, 27] Although the reflexes were not further denoted in literature,

an hexagonally ordered mesoporous structure of the tantalum oxide was suggested.[27] A know example for a hexagonally ordered mesoporous silica is so called SBA-15.[37, 38] Adopted from unit cell calculations for SBA-15,[39] the unit cell parameter of om-Ta_2O_5 was calculated to be 8.1 nm from X-ray diffraction data. This result is in line with reported unit cell data of ordered mesoporous Ta_2O_5.[26] A TEM study showed the ordered mesoporosity of the sample (**Figure 1b**). The sample consisted largely of particles with ordered mesoporous structure. From TEM micrographs, the pore diameter and wall thickness of om-Ta_2O_5 were identified to have be around 3 nm and 5 nm, respectively. These values are in agreement with previously reported parameters of ordered mesoporous Ta_2O_5.[26]

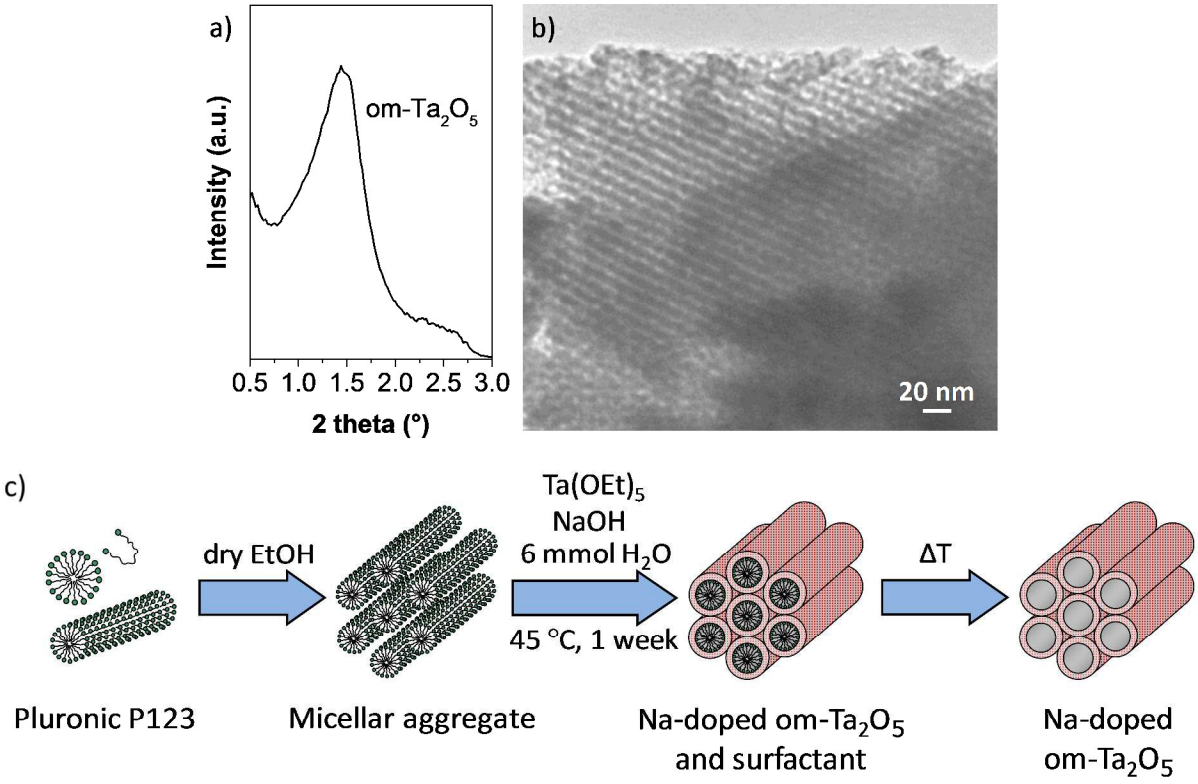

Figure 1. a) Low angle XRD pattern, and b) TEM image of om-Ta_2O_5, and c) preparation scheme of om-TaNa. After micelle formation of P123 in dry ethanol, tantalum ethoxide, sodium hydroxide and a small amount of water were added. The mixture was dried over 1 week at 40 °C before the template was removed by calcination and ordered mesoporous sodium loaded tantalum oxide was obtained.

Ordered mesoporous Ta_2O_5 is prepared under acidic conditions by using $TaCl_5$ as starting precursor.[26, 27] Herein, this synthetic methodology is modified by replacing the acidic conditions with basic conditions by using NaOH and tantalum ethoxide ($Ta(OEt)_5$) as precursor. According

to the reported synthesis of om-Ta_2O_5, a small amount of H_2O was added to the reaction to initiate hydrolysis of the precursor. As illustrated in **Figure 1c**, NaOH is added during the hydrolysis of $Ta(OEt)_5$ to achieve a homogeneous distribution of sodium in the tantalum oxide network. Usage of NaOH has two benefits: first, as a base it catalyzes the hydrolysis reaction of $Ta(OEt)_5$,[40] and second it provides Na that can be incorporated into the structure to form a sodium tantalate compound. Structures with different Na/Ta ratios could easily be obtained by changing the amount of NaOH. Thus, different samples were prepared that were labelled as om-TaNaX, with X being the atomic ratio of Ta/Na. The sample series consisted of Ta/Na ratios of 21, 9, 5 and 3, denoted accordingly as om-TaNa21, om-TaNa9, om-TaNa5 and om-TaNa3. The Ta/Na ratios were derived from the ideal case of producing amorphous samples with mixed Ta_2O_5 and $NaTaO_3$ phases. For example, the ratio of Ta/Na 21 results from a compound with a 10 Ta_2O_5 – 1 $NaTaO_3$ phase mixture. Other ratios were calculated accordingly. All samples of the series were amorphous as determined by wide angle XRD analysis (**SI Figure 1**).

The ordered structure of all om-TaNa samples was confirmed by low angle XRD analysis (**Figure 2a**). All patterns show a distinctive, yet broad reflex at similar 2θ values. It is worth mentioning that one reflex was observed for the om-TaNa samples, whereas om-Ta_2O_5 shows an additional reflex. This result suggested that the om-TaNa samples have an ordered porosity, which was denoted before as a worm-like structure.[26, 27] Compared to om-Ta_2O_5, the reflex of the om-TaNa samples was shifted to smaller 2θ values, indicating a bigger unit cell. In comparison to the unit cell parameter of om-Ta_2O_5 (8.1 nm), the unit cell parameter values of om-TaNa21, om-TaNa9, om-TaNa5 and om-TaNa3 increased to 11.4, 11.6, 11.6 and 12.3 nm, respectively. It should be considered that this calculation is vague, as the reflex of the om-TaNa samples is broad, but it underlines the trend that the addition of sodium led to an increase in unit cell size, which could be related to a change in pore size and wall thickness of the material. The increase in pore size and unit cell of a mesoporous ordered material due to the addition of ions was studied in detail for SBA-15.[41] Due to the interaction of different NaCl concentrations with P123 micelles in solution, the silica prepared by soft templating around these micelles exhibit increasing pore size and unit cell parameters with increasing salt concentration.[41] Although the observed trend, denoted as salt effect, was attributed predominantly to the interaction of Cl^- ions with the micelles, we expect the presence of NaOH to have similar influence.

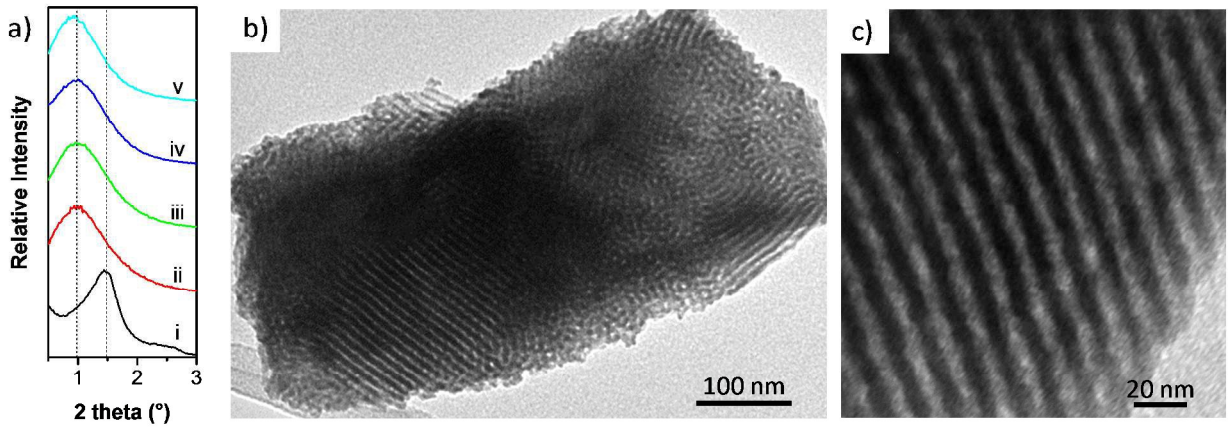

Figure 2. (a) Low angle XRD patterns of (i) om-Ta_2O_5, (ii) om-TaNa21, (iii) om-TaNa9, (iv) om-TaNa5 and (v) om-TaNa3, and TEM (b) and HR-SEM (c) images of om-TaNa9.

Low angle XRD confirmed the successful preparation of ordered mesoporous composite materials by using a novel method of soft-templating under basic conditions even at a high Ta/Na ratio of 3. Further increase of the NaOH amount (Ta/Na = 1) was also tested, but resulted in bulk particles instead of a mesoporous structure (data is not included here). The incorporation of sodium into the structure, from a diluted (Ta/Na = 21) up to a high (Ta/Na = 3) sodium amount, formed most likely an amorphous Na-loaded Ta_2O_5 composite material that exhibit an ordered structure. A higher sodium amount (Ta/Na = 1) will most likely lead to a $NaTaO_3$-like structure that could not be obtained as an ordered mesoporous structure through the same experimental conditions. The samples were further examined by TEM and the image of om-TaNa9 is presented in **Figure 2b**, showing the worm-like pore structure of the sample, which made up the majority of the pore structure of all om-TaNa samples. A detailed TEM survey revealed also the presence of hexagonal ordered mesoporosity in the sample (**Figure 2b-2c**), although these domains with hexagonal ordered porosity are often paired with domains of worm-like structure. From the TEM survey and a HR-TEM investigation the pore diameter and the wall thickness of om-TaNa9 were determine to be about 4 and 8 nm, respectively. In order to display the structure of om-TaNa9, the sample was further analyzed by SEM. The cross-sectional TEM and SEM images of the sample are given in **SI Figure 2. T**he high porosity throughout the particles is evident, which is presented in bright field STEM mode **(SI Figure 2b)**. A SEM image of the powdered material (**SI Figure 2c**) shows an irregular structure of pores at the particle surface. Through electron microscopy study we can show that the pore structure of the om-TaNa series consists of domains

of hexagonal ordered structure and worm-like structure, which is in agreement with low angle XRD analysis. The change in pore structure from hexagonal ordered mesoporosity in om-Ta_2O_5 to mainly worm-like mesoporosity in om-TaNa samples is a consequence of the change in P123 micelle geometry. As the micelles form hexagonally arranged rods in the synthesis of om-Ta_2O_5, they deform during the synthesis of om-TaNa to arrange as worm-like geometry. Similar to the salt effect,[41] the addition of ions to the micelle solution can influence the size and shape of the micelles,[42] thus we believe the formation of worm-like micelles was caused by the presence of Na^+ and OH^- ions in the starting solution.

After the structural investigation by XRD and TEM analysis, the materials were further characterized by N_2-physisorption analysis. The isotherms and pore size distributions of om-Ta_2O_5, and the om-TaNa samples are plotted in **Figure 3** and an overview of the textural parameters is given in **Table 1**. All samples show type IV isotherms that are characteristic for mesoporous materials.[38, 43] Compared to om-Ta_2O_5, which shows a narrow hysteresis, om-TaNa samples have a capillary condensation step from 0.4 to 0.7 P/P_0. The pore size of the samples increased with Na-doping, as it can be seen from the **inset in Figure 3**.

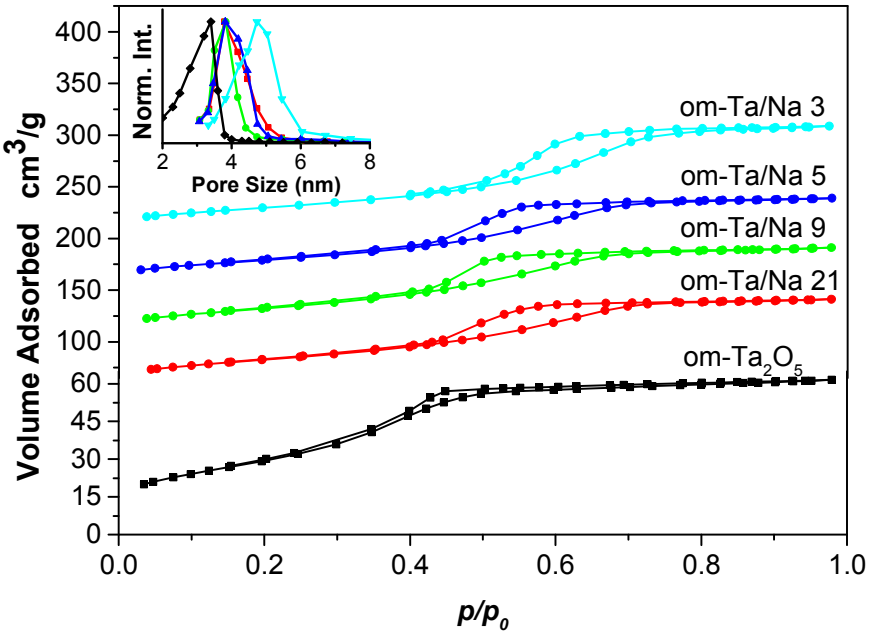

Figure 3. N_2-physisorption isotherms of om-Ta_2O_5 and sodium loaded ordered mesoporous tantalum oxides. The isotherms have an offset of 50 cm^3 g^{-1}. The inset shows the pore size distribution of the samples calculated from the N_2-physisorption desorption branch.

Om-Ta_2O_5 contained the smallest pores of 3 nm, while om-TaNa21 om-TaNa9 and om-TaNa5 showed 4 nm pores and om-TaNa3 had pores of 5 nm, which is in good agreement with TEM analysis. The increase in pore size could be the reason for the increase of unit cell size as it has been calculated from low angle XRD analysis. Additionally, the wall thickness (h_w) of the ordered structure can be calculated from the measured pore diameter d_0 and the unit cell parameter a ($h_w = a - d_o$).[26] Accordingly, the wall thickness of om-Ta_2O_5 was calculated to be 4.7 nm. This value is in good agreement with the wall thickness determined by TEM analysis (5 nm). For the om-TaNa samples the wall thickness increased with increasing sodium content, giving a wall thickness of 7.6, 7.8, 7.8 and 8.1 nm for om-TaNa21, om-TaNa9, om-TaNa5 and om-TaNa3, respectively. The estimated wall thickness is in good agreement with the TEM analysis, which displayed a wall thickness of 8 nm for all om-TaNa samples. A higher wall thickness can be caused by increasing the metal ion concentration in the synthesis solution, as it has been observed before for ordered mesoporous Ta_2O_5.[27] In this sample series, the ion concentration was increased due to the addition of sodium during the synthesis, which led to the increase in wall thickness. Following the same trend, the pore volume increased from 0.09 to 0.17 $cm^3\ g^{-1}$ along with the increased sodium loading. However, the surface area remained moderately constant for all samples in the range of 110 to 120 $m^2\ g^{-1}$. In summary, the XRD, TEM, and N_2-physisorption data showed the formation of om-TaNa samples via a novel soft-templating route. The om-TaNa samples exhibit an ordered mesoporous structure similar to that of om-Ta_2O_5, but form a larger unit cell compared to that of om-Ta_2O_5 due to a larger pore size and wall thickness.

Following the qualitative study on structure and morphology of the om-TaNa samples, the Ta/Na ratios were examined by energy-dispersive X-ray spectroscopy (EDX) analysis (SI Table 1). As determined, the Ta/Na ratios of om-TaNa21, om-TaNa9, om-TaNa5 and om-TaNa3 were 24.6, 9.4, 6.7 and 3.5, respectively, showing that the prepared samples are in agreement with the theoretical values. In order to determine the oxidation state of tantalum in the amorphous samples, om-Ta_2O_5 and om-TaNa9 were investigated by X-Ray photoelectron spectroscopy (XPS) analysis, a surface sensitive analysis technique. The binding energies of om-Ta_2O_5 were located at 28.1 and 26.2 eV for Ta $4f_{5/2}$ and $4f_{7/2}$, respectively (**SI Figure 3**). Compared to reported values for tantalum oxide these values are at higher energies.[44] However, they are in good agreement with previously reported binding energies for amorphous tantalum oxide with oxidation state +5.[32] In comparison, om-TaNa9 showed the same Ta 4f binding energies (28.1

and 26.2 eV for Ta $4f_{5/2}$ and $4f_{7/2}$, respectively). In addition, the sample had a distinct Na 1s peak at a binding energy of 1071.5 eV (spectrum not included). The binding energies for Ta 4f of the Na-containing sample are analogue to the Ta 4f binding energies of om-Ta_2O_5. Further, the Ta/Na ratio was analyzed by XPS. Different from the theoretical value (Ta/Na = 9), a slightly higher Na concentration was found at the surface of om-TaNa9 by XPS, giving a Ta/Na = 7. These results indicate that most of the Na^+ is not incorporated into the Ta_2O_5 crystal structure as the Ta 4f binding energies for om-TaNa9 and om-Ta_2O_5 are identical. A more plausible location for the Na ions would be at the surface of the sample through coulomb adsorption, which is supported by the XPS results indicates a higher Na^+ concentration (XPS: Ta/Na = 7) at the surface than the overall Na^+ concentration (theoretical: Ta/Na = 9; EDX: Ta/Na = 9.4). As mentioned before, the addition of NaOH increases the pore size and unit cell size due to the salt effect on the P123 micelles. Due to the ionic interactions, Na^+ ions would be closely located at the polar surface of the P123 micelles. These Na^+ ions will thus be situated in the surface of the Ta_2O_5 network that is formed around these micelles. Therefore, the majority of the Na^+ ions should be located at the surface or close to the surface of the om-TaNa samples, probably through coulomb interaction as there was no shift in Ta 4f binding energies detected via XPS. One should keep in mind that the XPS is a surface sensitive technique, thus the incorporation of Na into the structure of the Ta_2O_5 cannot be excluded although there is not a significant shift of the peak positions.

Table 1. Textural parameters and hydrogen evolution rates of om-Ta_2O_5 and sodium loaded ordered mesoporous tantalum oxides.

sample	Pore volume ($cm^3\ g^{-1}$)	Pore size (nm)	Surface area ($m^2\ g^{-1}$)	Band gap energy (eV)[a]	H_2 rate ($\mu mol\ h^{-1}$)[b]
om-Ta_2O_5	0.09	3	108	4.1	642
om-TaNa21	0.14	4	121	4.2	967
om-TaNa9	0.14	4	120	4.3	1359
om-TaNa5	0.14	4	108	4.2	1237
om-TaNa3	0.17	5	110	4.2	1317
c-Ta_2O_5	n.a.	n.a.	1	4.0	438

[a]Determined from Tauc plots for indirect semiconductor. [b]Hydrogen evolution from 10 vol-% methanol/water solution.

In order to gain more information concerning the location of the Na, a deeper investigation of the samples was conducted by using Raman spectroscopy. This analytical method can give insight about bulk structural organization of materials.[45, 46] We investigated the Raman shifts of Ta-O polyhedra in om-Ta_2O_5, om-TaNa sample series and reference samples c-Ta_2O_5 and SS-$NaTaO_3$ (prepared via solid state reaction). The Raman spectrums of materials are giving in **SI Figure 4** where a clear a trend in the om-TaNa sample series with increasing Na-content in the range of 700-560 cm^{-1} can be observed. Above 400 cm^{-1}, Raman signals are considered stretching and torsional modes of Ta-O polyhedra. The Raman signals of reference c-Ta_2O_5 show both bipyramidal pentagonal and octahedral coordination of TaO_7 and TaO_6 at 840 cm^{-1} and triply split peaks (indicated by circles) appear in the range of 700-560 cm^{-1}, respectively.[47] The signals below 400 cm^{-1} are regarded as interpolyhedral Ta-O-Ta bending and Ta-Ta vibration.[47] In comparison, amorphous om-Ta_2O_5 displays a broad TaO_6 peak in the same wave number region as c-Ta_2O_5 (700-560 cm^{-1}), which was also reported earlier for amorphous tantalum oxide.[48] Furthermore, the full spectrum of om-Ta_2O_5 is in good agreement with reported Raman data for amorphous tantalum oxide.[48] With increasing Na-content, the center of the TaO_6 peak shifts to lower wave numbers from 660 to 635 cm^{-1}. As reported in the literature, [46, 49] SS-$NaTaO_3$ shows Na^+ modes < 240 cm^{-1} and TaO_6 modes above 240 cm^{-1} with the main peak observed at 620 cm^{-1}. In comparison, nanocrystalline $NaTaO_3$ shows a broad peak in the region of about 550-700 cm^{-1} with a maximum at 600 cm^{-1}.[45] Therefore, the peak shift of the om-TaNa samples from 660 to 635 cm^{-1} might indicate a formation of a $NaTaO_3$-like sub-structure dispersed in the main tantalum oxide network due to the incorporation of small amounts of Na^+ into the core structure. Alternatively, the shift could indicate an organization of the amorphous tantalum oxide network, which increases with increasing Na-content. This organization has been observed for amorphous tantalum oxide films above 600 °C.[46] As the om-TaNa samples were treated at 550 °C, this result could indicate that Na^+ ions act as a flux, allowing the structure to organize at lower temperature. Both cases strongly suggest that at least some quantity of the added Na^+ ions is incorporated into the core of the structure and this changes the atomic structure compared to om-Ta_2O_5.

We examined the composition of the samples and proved that the ordered mesoporous structure was successfully retained along the series. Afterwards, the influence of Na on the band gap energy (E_g) of the materials was investigated, which is a key property for photocatalytic

applications. The band gaps were determined via Tauc plots for indirect semiconductors[50] (**Figure 4)** and the energy values are presented in **Table 1**. The corresponding UV-Vis spectra are shown in **SI Figure 5**. Starting with om-Ta_2O_5, the amorphous sample showed a band gap of 4.1 eV, which is similar to the highly crystalline c-Ta_2O_5 with a 4.0 eV band gap.[51] The addition of sodium to the material altered the E_g towards higher energies. As determined for om-TaNa21, the band gap increased to 4.1 eV. Further addition of sodium caused an additional increase in band gap energy. The highest band gap was determined for om-TaNa9 with band gap energy of 4.3 eV. The following samples with higher Na amount, namely om-TaNa5 and om-TaNa3 had an E_g value of 4.2 eV. The increase of band gap energy could be related to the presence of sodium in the structure, which led to the formation of an amorphous ordered mesoporous Na-loaded Ta_2O_5 composite sample and thus altered the energetic structure, as it was shown for Fe-doped into om-Ta_2O_5.[52] The incorporation of Na^+ ions into the structure was also suggested by Raman spectroscopy, which is in agreement with the change in band gap energy with increasing Na-loading. Further, structural parameters like pore size and unit cell of the ordered porous system where changed with the addition of sodium, which could influence the electronic structure and band gap as well.

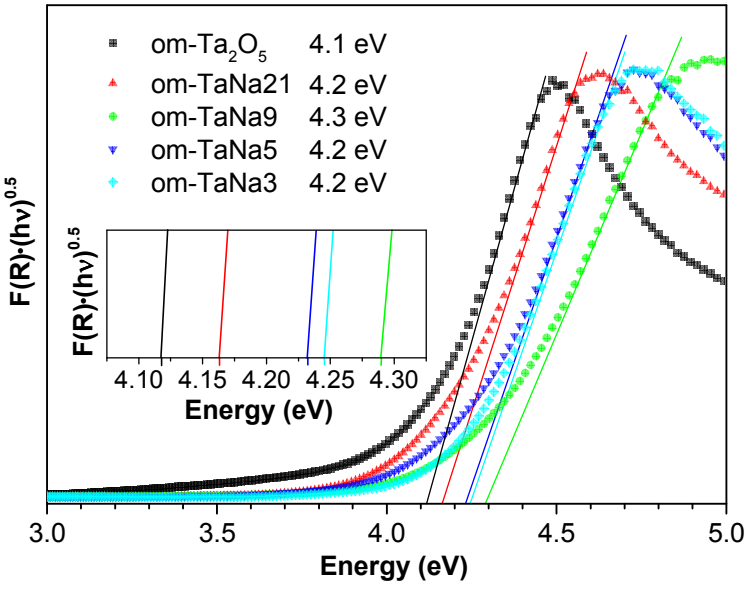

Figure 4. Tauc plots of om-Ta_2O_5 and the sample series of om-TaNa (inset: close-up of intersection with x-axis).

After the detailed characterization of the materials, the photocatalytic performance towards water splitting was tested. Therefore, the om-TaNa samples were illuminated for 2 h under UV light in a 10 vol-% methanol/water mixture. The obtained hydrogen evolution rates are displayed in **Figure 5**. It is noticeable that all ordered mesoporous samples showed a higher activity than the highly crystalline c-Ta_2O_5, which produced 438 µmol h^{-1} of hydrogen, although the ordered mesoporous samples have an amorphous structure. The higher activity is related to the higher surface area and nanostructured morphology of the ordered, mesoporous materials. These features are beneficial for photocatalysis as a high surface area offers a high number of active sites for water splitting and generated charge carriers have short diffusion paths due to the nanostructured morphology. Furthermore, all om-TaNa samples showed a higher H_2 generation rate than om-Ta_2O_5 (642 µmol h^{-1}) although the surface areas of om-Ta_2O_5 and the om-TaNa samples are very similar. Thus, the enhanced activities of the om-TaNa samples derive from the incorporation of Na, which allows the formation of an ordered mesoporous Na-loaded Ta_2O_5 composite structure that could provide a platform for junctions. In fact, sodium tantalates are more active in photocatalytic water splitting than Ta_2O_5,[17] and an incorporation of Na^+ into the tantalum oxide structure is practicable, as confirmed by Raman spectroscopy.

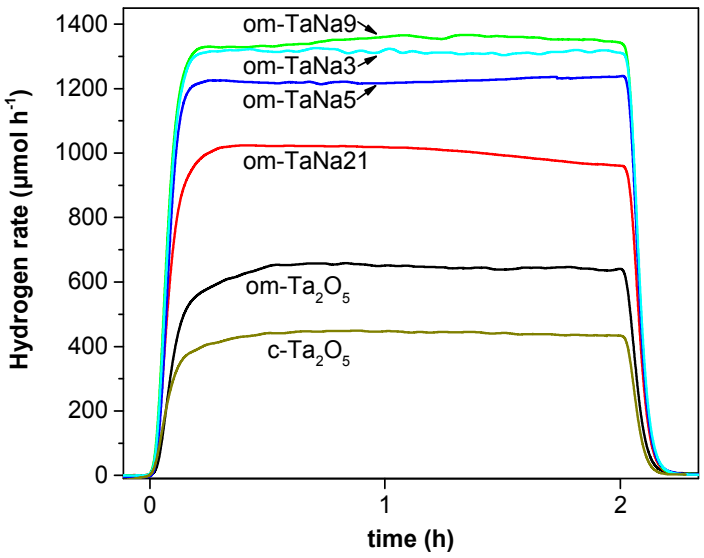

Figure 5. Hydrogen generation rates of ordered mesoporous tantalum oxide (om-Ta_2O_5) and series of sodium loaded om-Ta_2O_5 (om-TaNa). Hydrogen evolution was tested in 10 vol-% methanol/water solution.

The om-TaNa21 sample, containing the lowest amount of sodium, reached a hydrogen generation rate of 967 µmol h^{-1}, whereas om-TaNa5 and om-TaNa3 produced H_2 in rates of 1237 and 1317 µmol h^{-1}, respectively. The highest rate however was achieved with a Ta/Na ratio of 9, which can be attributed to the band gap energy, as it was the highest of the series (4.3 eV). If an electron is excited over a higher band gap into the conduction band, also the reactivity of the excited electron would be higher compared to the reactivity of an electron being excited into a lower conduction band. Therefore, om-TaNa9 showed slightly higher activity for hydrogen production than the other samples of the series. Indeed, recent research has shown that a small change in band gap and shift in conduction band energy of CdSe nanocrystals result in elevated hydrogen production rates due to thermodynamics and kinetics of the hydrogen evolution reaction.[53] After two hours, om-TaNa9 was generating hydrogen at the rate of 1359 µmol h^{-1}. This exceeded the hydrogen production of c-Ta_2O_5 by a factor of 3, proofing that the activity of an amorphous material with a high surface area can surpass the activity of its crystalline counterpart. In conclusion, om-Ta_2O_5 showed higher activity than c-Ta_2O_5 due to a higher surface area and nanostructured morphology, providing short diffusion paths for charge carriers to the surface. The incorporation of Na^+, leading to om-TaNa samples further enhanced the activity while retaining porosity and a high surface area.

As the om-TaNa9 sample showed the highest activity among all samples, a series of samples with other cations in the ratio of Ta/X = 9 was prepared in order to check the applicability of the preparation method. For this purpose, K, Ca, Ba and Sr were used as X, as they show photocatalytic activity when they form mixed oxides with tantalum.[13-15] For this purpose, NaOH was replaced during the synthesis by the respective K, Ca, Ba and Sr hydroxide precursors. As it was observed via low angle XRD analysis (**SI Figure 6a**), om-TaK9 showed a reflex at 0.9° 2θ slightly lower than the reflex of om-TaNa9, indicating a successful synthesis of a worm-like porosity, whereas om-TaCa9 and om-TaBa9 showed only a very broad reflex at lower angle. For the Sr-incorporated sample no low angle diffraction peak was observed. Thus, the formation of om-TaK9 could be confirmed via low angle XRD, while the synthesis of om-TaCa9, om-TaBa9 and om-TaSr9 showed a poorly ordered or unordered structure. Next to low angle XRD, the BET surface area of om-TaK9 was determined to be 121 m^2 g^{-1}, being close to the value of om-TaNa9 (120 m^2 g^{-1}). In contrast, the samples with Ca, Ba and Sr showed low surface areas of 6, 12 and 5 m^2 g^{-1}. These results confirm that the addition of Ca, Ba and Sr do not yield

an ordered mesoporous structure. An additional TEM analysis of om-TaCa9, om-TaBa9 and om-TaSr9 showed bulk particles with a dense morphology (not shown here), underlining the findings of the XRD and N_2-physisorption analyses. Concerning the influence on the band gap energies of the materials, the E_g values were estimated from Tauc plots for the om-TaX9 samples (**SI Figure 6b**). In contrast to om-TaNa9, the om-TaX9 samples with X = K, Ca, Ba and Sr have a band gap of 4.2 eV. The photocatalytic hydrogen production rate of the sample series was determined as described before. As it is shown in **SI Figure 6c**, om-TaNa9 had the highest activity of the series. The incorporation of K led to a H_2 rate of 975 µmol h^{-1} which was double the activity of om-Ta_2O_5. On the other hand, Ca, Sr and Ba-addition showed H_2 production rates of 228, 255 and 246 µmol h^{-1}, which were below the activity of om-Ta_2O_5. We conclude that the incorporation of alkali metal ions yield an ordered mesoporous structure with a high surface area (120 m^2 g^{-1}) and lead to an enhancement of the photocatalytic activity towards photocatalytic hydrogen production. In contrast, divalent cations have no positive effect on the activity of amorphous om-Ta_2O_5. Moreover, the ordered structure cannot be obtained and the samples exhibit a low surface area. As mentioned before, the addition of ions to the micelle solution can alter the size and shape of the micelles. Therefore om-TaNa samples and om-TaK exhibited a mainly worm-like porosity, while om-Ta_2O_5 showed a mainly hexagonal ordered porosity. In the case of adding Ca^{2+}, Ba^{2+} and Sr^{2+} to the micelle solution, the influence of these divalent cations may cause the micellar structure to collapse. Therefore, there was hardly any ordered porosity observed via low angle XRD. Further, the earth alkaline metals may cause a more rapid hydrolysis of the tantalum oxide network, obstructing a decent replication of micellar aggregates. These factors can be the reason why the addition of earth alkaline metals did not yield ordered mesoporous structures.

The ultimately desired reaction in photocatalysis is overall water splitting. However, without the use of any co-catalyst, Ta_2O_5 cannot generate measurable amounts of hydrogen and oxygen.[33] As a step to increase the photocatalytic activity of om-TaNa9 towards water splitting, the sample was loaded with various amounts of NiO_x as a co-catalyst. The NiO_x co-catalyst represents the combination of Ni and NiO, which was prepared according to literature.[31] The NiO_x-loaded sample was analyzed by STEM, and an elemental mapping showed a fine dispersion of Ni in the sample (**SI Figure 7**). In order to obtain a high Ni signal, the elemental mapping was performed on the sample with the highest NiO_x-loading (5 wt-%). Additionally, the sample showed a fine distribution of Na throughout the sample, indicating a well-dispersed incorporation

of Na during the synthesis. The NiO_x co-catalyst functions as a Schottky contact and traps electrons that promote the reduction of water to hydrogen. To investigate the optimum co-catalyst loading for amorphous om-TaNa9, four different loadings were attempted (0.5, 1, 2.5 and 5 wt-% NiO_x) and the hydrogen evolution rates were first screened with methanol as a sacrificial agent (**Figure 6**). As seen in **Figure 6a**,as-made om-TaNa9 showed a hydrogen rate of 1359 µmol h^{-1}, while 0.5 and 1 wt-% NiOx loading led to an increase to 1624 and 2007 µmol h^{-1}. Higher loading of 2.5 wt-% NiO_x led to the maximum H_2 rate of 2370 µmol h^{-1}. With further increasing the co-catalyst loading to 5 wt-% the activity dropped down to 2110 µmol h^{-1}. This is shown in **Figure 6b**, where hydrogen production rates are presented over NiO_x loading. This trend is known for photocatalysts with high co-catalyst loadings. The addition of a co-catalyst is beneficial until the loading amount masks the surface sites of the photocatalyst, thus reducing the photocatalytic activity.[31, 54]

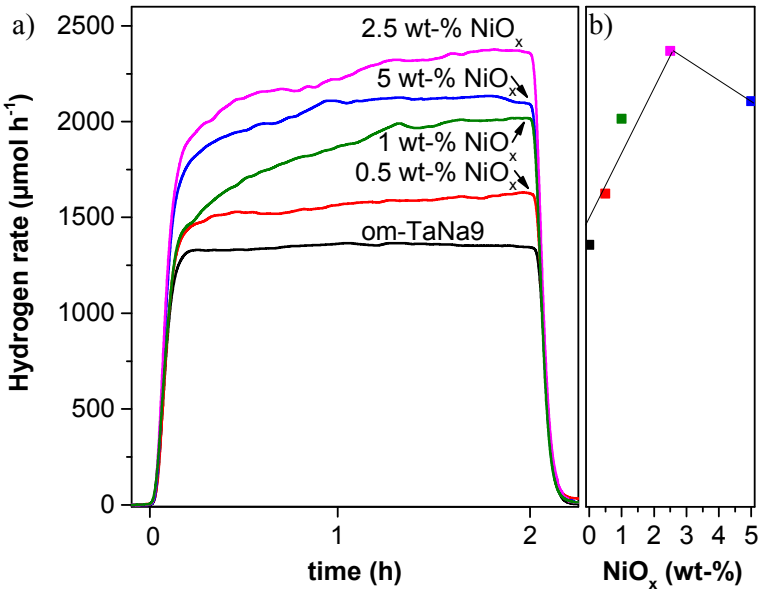

Figure 6. a) Hydrogen evolution rates of amorphous om-TaNa9 with different loading amounts of NiO_x tested over 2h irradiation. b) H_2 production rates presented over NiO_x loading of om-TaNa9. Hydrogen generation was tested in 10 vol-% methanol/water solution.

After the screening, photocatalytic overall water splitting was conducted on the most active material om-TaNa9 with 2.5 wt-5 NiO_x loading. During the reaction, the sample was

irradiated for 30 h in the reactor in pure water. After 16 h, hydrogen and oxygen were produced with stable and stoichiometric rates. In **Figure 7**, the cycling of the sample over the final 14 h is presented. The first three cycles show the gas evolution rates of 2 h irradiation, ending with a fourth cycle of 8 h irradiation. Between the cycles, the set-up was purged with Ar in the dark to remove any traces of hydrogen and oxygen. In total, the sample generated an average of 64 µmol h^{-1} hydrogen and 31 µmol h^{-1} oxygen with decent stability. For comparison, om-TaNa9 without co-catalyst was also tested for overall water splitting. The sample generated hydrogen at a production rate of about 13.3 µmol h^{-1} with non-stoichiometric amounts of oxygen. This behavior has been also observed for Ta_2O_5 with insufficient amount of co-catalyst due to low activity to accomplish overall water splitting.[31, 33, 55] In comparison to om-TaNa9 with 2.5 wt-% NiO_x, the sample without co-catalyst generated around 5 times less hydrogen in overall water splitting. Thus, the decoration of NiO_x is necessary for overall water splitting with om-TaNa9.

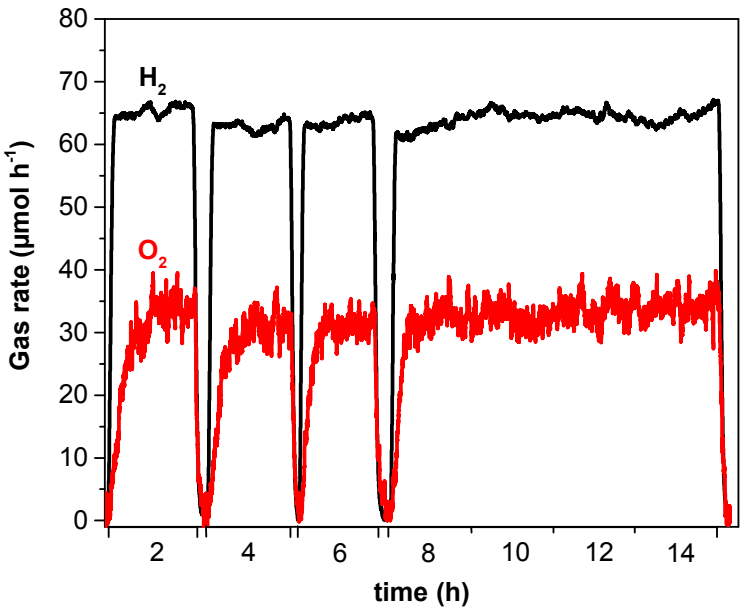

Figure 7. Overall water splitting of amorphous om-TaNa9 loaded with 2.5 wt-% NiO_x under UV irradiation for 14 h. The reaction was cycled three times over 2h. At last, the sample was irradiated for 8h. After each cycle the lamp was switched off and the system was purged with Ar.

To evaluate the activity of the new catalyst system consisting of Na-loaded om-Ta_2O_5 samples, we compared the activity of prepared materials with previously reported amorphous

mesoporous tantalates. It should be kept in kind that a precise comparison is tough, since mostly different photocatalytic reaction conditions (reactor volume, catalyst concentration, light source) are used. Firstly, om-TaNa9 is compared with Ta_2O_5 that is prepared via sol-gel synthesis.[56] The amorphous samples had comparable surface areas to our om-TaNa series of 133– 80 m^2 g^{-1}. The photocatalytic activity of these samples was tested in 10 vol-% methanol aqueous solution with a catalyst concentration of 1 g L^{-1} (200 mg of catalyst) under UV light illumination from a 300 W Hg high pressure lamp. The amorphous samples produced hydrogen rates far below 100 µmol h^{-1} g_{cat}^{-1}. In contrast, our most active sample (om-TaNa9) produced hydrogen at a rate of 13000 µmol h^{-1} g_{cat}^{-1}, when calculating to the same unit. It needs to be emphasized that a direct comparison is questionable since we have different photocatalytic reaction conditions. (10 vol-% methanol aqueous solution, 100 mg catalyst, 0.5 g L^{-1} catalyst concentration, 150 Hg middle pressure lamp).

The hydrogen production rate from overall water splitting of om-TaNa9 with 2.5 wt-% NiO_x was compared to hydrogen production rates from literature of other amorphous tantalates. An amorphous mesoporous Ta_2O_5 that was prepared via soft-templating showed a hydrogen production of 65.7 µmol g^{-1} h^{-1} (no O_2 detected, 50 mg of catalyst in 30 mL water = 1.7 g L^{-1}, 300 W Xe lamp).[20] Therein, the Ta_2O_5 was calcined at 500°C and 1.5 wt-% NiO was used as a co-catalyst. Compared to our set-up (100 mg catalyst, 0.5 g L^{-1}, 150 Hg middle pressure lamp) the om-TaNa9 with 2.5 wt-% NiO_x, which would calculate to a rate of 640 µmol g^{-1} h^{-1}, the novel material presented here is ten times more active than the previously reported ordered mesoporous tantalum oxide. However, it is important to consider that the reported catalyst was illuminated by a 300 W Xe lamp, which emits a limited amount of UV photons above 4.0 eV whereas we used a mercury lamp with UV emission. Furthermore, the hydrogen production rate was given in µmol g^{-1} h^{-1}, although only 50 mg of catalyst were measured. Thus, the comparison is limited. In another report, the structure of a mesoporous tantalum oxide was loaded during the synthesis with Ni in a Ta/Ni ratio of 9 and then calcined at 600 °C for 1 h to activate it prior to the photocatalytic test.[34] The reported hydrogen and oxygen rates were 68 and 38 µmol h^{-1}, respectively. Although the rates are very similar to om-TaNa9 with 2.5 wt-5 NiO_x, in previous report a stronger lamp (450 W Hg high pressure lamp; our lamp: 150 W Hg middle pressure lamp), and a higher catalyst concentration (350mg of catalyst in 420 mL water = 0.8 g L^{-1}; our catalyst concentration: 0.5 g L^{-1}) was used.

Since the material was investigated in a long-term overall water splitting test, the structural ordering and atomic composition were investigated afterwards by low angle XRD and EDX. Before the catalytic reaction, atomic ratios of om-TaNa9 with 2.5 wt-% NiO_x were measured as Ta/Na = 10.3 and Ta/Ni = 13.8. Prior to NiO_x loading, the Ta/Na ratio was 9.4 for om-TaNa9. These values are comparable with each other, given the limitations of the EDX analysis. The theoretical atomic Ta/Ni ratio is 14.8, calculated for 2.5 wt-% NiO loading and a Na-loaded Ta_2O_5 composite with Ta/Na = 9. The measured value (13.8) is in the range of the calculated number as well. After the catalytic test, the material was analyzed by EDX and it was found that the sodium and nickel content were reduced: the amount of Na was lowered by 66 % and the nickel content shrunk by 70%. The lowering of the two components is most likely due to the washing-out during the initial 16 h of the long-term overall water splitting test, where hydrogen and oxygen were produced non-stoichiometrically. We assume that sodium can leave the material from positions close to the surface easily as the sample is not crystalline, which leads to the reduced Na content after the overall water splitting test. Recently, the corrosion of a NiO_x co-catalyst was demonstrated, which explains the loss of Ni after the catalytic test.[57] Since the catalytic test altered the atomic composition of the catalyst, the stability of the ordered porosity was studied by low angle XRD. **SI Figure 8** shows the low angle XRD patterns of om-TaNa9 with 2.5 wt-% NiO_x loading before and after the long-term overall water splitting test. The reflex intensity and position are similar for both samples, indicating a retained structure throughout the water splitting reaction.

Conclusion

With a modified synthetic approach, a series of amorphous tantalates with different amount of alkali and alkaline earth metals was prepared. The incorporation of Na and K resulted in an ordered mesoporous structure while the ordered mesoporous structure was not obtained with the addition of Ca, Ba and Sr. Among those tantalates, Na and K-based materials displayed a much better water splitting performance in comparison to ordered mesoporous Ta_2O_5. By varying the amount of Na, a series of sodium tantalate composites was synthesized. In a photocatalytic test, the theoretical ratio of Ta/Na = 9 showed the highest activity towards water splitting, which was attributed to incorporation of Na to core structure of Ta_2O_5. The performance of this material was further enhanced with a NiO_x co-catalyst loading, where a loading amount of 2.5 wt-% NiO_x

was found to be the optimal amount. Even though sodium and nickel were partly washed out from the material after long-term overall water splitting, ordered porosity and activity towards water splitting were retained. After 30h of irradiation, the amorphous om-TaNa9 loaded with 2.5 wt-% NiO_x was able to split water into H_2 and O_2 at stable rates of 64 and 31 µmol h^{-1}, respectively. These results show that amorphous materials with a high surface area can split water into hydrogen and oxygen and small amounts of sodium or potassium can alter structural parameters and influence the photocatalytic activity of tantalates.

Acknowledgement

We thank Dr. C. Weidenthaler for XPS analyses, Prof. Dr. C. Lehmann and B. Spliethoff for electron microscope analyses (HR-TEM, STEM and element mapping), and S. Palm for EDX analyses. We are grateful to Dr. M. Meggouh for helpful discussions on the manuscript. Gratitude to Ocean Optics supplying the Raman spectrometer. In addition, we thank Max-Planck-Society and Fonds der Chemischen Industrie (FCI) for funding. This work was partly supported by Cluster of Excellence RESOLV (EXC 1069) funded by the Deutsche Forschungsgemeinschaft (DFG). T.G. thanks FCI for a Chemiefonds Fellowship.

References

1. T. Hisatomi, J. Kubota and K. Domen, *Chem. Soc. Rev.*, 2014, **43**, 7520-7535.
2. E. E. Benson, C. P. Kubiak, A. J. Sathrum and J. M. Smieja, *Chem. Soc. Rev.*, 2009, **38**, 89-99; T. Hisatomi, K. Takanabe and K. Domen, *Catal. Lett.*, 2015, **145**, 95-108; D. Kim, K. K. Sakimoto, D. Hong and P. Yang, *Angew. Chem. Int. Ed.*, 2015, **54**, 3259-3266.
3. Y. Tachibana, L. Vayssieres and J. R. Durrant, *Nat. Photon.*, 2012, **6**, 511-518; X. Li, J. Yu, J. Low, Y. Fang, J. Xiao and X. Chen, *J. Mater. Chem. A*, 2015, **3**, 2485-2534; M. Kitano and M. Hara, *J. Mat. Chem.*, 2010, **20**, 627-641; E. Nurlaela, S. Ould-Chikh, M. Harb, S. del Gobbo, M. Aouine, E. Puzenat, P. Sautet, K. Domen, J.-M. Basset and K. Takanabe, *Chem. Mater.*, 2014, **26**, 4812-4825.
4. R. van de Krol, Y. Liang and J. Schoonman, *J. Mater. Chem.*, 2008, **18**, 2311-2320.
5. H. M. Chen, C. K. Chen, R.-S. Liu, L. Zhang, J. Zhang and D. P. Wilkinson, *Chem. Soc. Rev.*, 2012, **41**, 5654-5671.
6. T. Grewe, M. Meggouh and H. Tüysüz, *Chem. - Asian J.*, 2015, DOI: 10.1002/asia.201500723.
7. F. E. Osterloh, *Chem. Soc. Rev.*, 2013, **42**, 2294-2320; F. Osterloh, *Top. Curr. Chem.*, 2015, DOI: 10.1007/128_2015_633; R. Abe, *J. Photochem. Photobio. C: Photochem. Rev.*, 2010, **11**, 179-209.
8. K. Takanabe, *Top. Curr. Chem.*, 2015, DOI: 10.1007/128_2015_646.
9. R. Marschall, *Top. Curr. Chem.*, 2015, DOI: 10.1007/128_2015_636; S. J. A. Moniz, S. A. Shevlin, D. J. Martin, Z.-X. Guo and J. Tang, *Energy Env. Sci.*, 2015, **8**, 731-759.
10. H. Tüysüz and C. K. Chan, *Nano Energy*, 2013, **2**, 116-123.
11. T. Grewe, K. Meier and H. Tüysüz, *Catal. Today*, 2014, **225**, 142-148.
12. K. Takanabe and K. Domen, *Green*, 2011, **1**, 313-322.

13. H. Kato and A. Kudo, *Chem. Phys. Lett.*, 1998, **295**, 487-492.
14. H. Kato and A. Kudo, *J. Phys. Chem. B*, 2001, **105**, 4285-4292.
15. H. Kato and A. Kudo, *Catal. Today*, 2003, **78**, 561-569.
16. A. Kudo and Y. Miseki, *Chem. Soc. Rev.*, 2009, **38**, 253-278.
17. P. Zhang, J. Zhang and J. Gong, *Chem. Soc. Rev.*, 2014, **43**, 4395-4422.
18. H. Kisch, *Angew. Chem., Int. Ed.*, 2013, **52**, 812-847; D. Wang, A. Pierre, M. G. Kibria, K. Cui, X. Han, K. H. Bevan, H. Guo, S. Paradis, A.-R. Hakima and Z. Mi, *Nano Lett.*, 2011, **11**, 2353-2357; J. Fonseca de Lima, M. H. Harunsani, D. J. Martin, D. Kong, P. W. Dunne, D. Gianolio, R. J. Kashtiban, J. Sloan, O. A. Serra, J. Tang and R. I. Walton, *J. Mater. Chem. A*, 2015, **3**, 9890-9898; J. Xu, C. Pan, T. Takata and K. Domen, *Chem. Commun.*, 2015, **51**, 7191-7194.
19. T. Wang, X. Meng, G. Liu, K. Chang, P. Li, Q. Kang, L. Liu, M. Li, S. Ouyang and J. Ye, *J. Mater. Chem. A*, 2015, **3**, 9491-9501; L. Guo, S. Ida, A. Takashiba, T. Daio, N. Teramae and T. Ishihara, *New J. Chem.*, 2014, **38**, 1392-1395.
20. L. Guo, H. Hagiwara, S. Ida, T. Daio and T. Ishihara, *ACS Appl. Mater. Interfaces*, 2013, **5**, 11080-11086.
21. H. Tüysüz, Y. Hwang, S. Khan, A. Asiri and P. Yang, *Nano Res.*, 2013, **6**, 47-54; T. Grewe, X. Deng and H. Tüysüz, *Chem. Mater.*, 2014, **26**, 3162-3168; Y. Zheng, L. Lin, X. Ye, F. Guo and X. Wang, *Angew. Chem., Int. Ed.*, 2014, **53**, 11926-11930.
22. B. Liu, L. Ning, H. Zhao, C. Zhang, H. Yang and S. Liu, *Phys. Chem. Chem. Phys.*, 2015, DOI: 10.1039/C5CP00450K; X. Ge, F. W. T. Goh, B. Li, T. S. A. Hor, J. Zhang, P. Xiao, X. Wang, Y. Zong and Z. Liu, *Nanoscale*, 2015, DOI: 10.1039/C5NR01272D; H. Cheng, J. Hou, O. Takeda, X.-M. Guo and H. Zhu, *J. Mat. Chem. A*, 2015, DOI: 10.1039/C5TA01864A.
23. M. Higashi, K. Domen and R. Abe, *Energy Env. Sci.*, 2011, **4**, 4138-4147.
24. H. Cui, G. Zhu, Y. Xie, W. Zhao, C. Yang, T. Lin, H. Gu and F. Q. Huang, *J. Mater. Chem. A*, 2015, DOI: 10.1039/C5TA01544H.
25. H. Tüysüz and F. Schüth, *Adv. Catal.*, 2012, **55**, 127-239.
26. P. Yang, D. Zhao, D. I. Margolese, B. F. Chmelka and G. D. Stucky, *Chem. Mater.*, 1999, **11**, 2813-2826.
27. K. Nakajima, M. Hara, K. Domen and J. N. Kondo, *Chem. Lett.*, 2005, **34**, 394-395.
28. J. N. Kondo and K. Domen, *Chem. Mater.*, 2008, **20**, 835-847.
29. U. Stutenbäumer, *Ethiop. J. Sci.*, 1999, **22**, 15-30.
30. M. W. Kanan and D. G. Nocera, *Science*, 2008, **321**, 1072-1075; A. Indra, P. W. Menezes, N. R. Sahraie, A. Bergmann, C. Das, M. Tallarida, D. Schmeißer, P. Strasser and M. Driess, *J. Am. Chem. Soc.*, 2014, **136**, 17530-17536.
31. Y. Takahara, J. N. Kondo, T. Takata, D. Lu and K. Domen, *Chem. Mater.*, 2001, **13**, 1194-1199.
32. T. Grewe and H. Tüysüz, *ChemSusChem*, 2015, **8**, 3084-3091.
33. K. Sayama and H. Arakawa, *J. Photochem. Photobio. A: Chem.*, 1994, **77**, 243-247.
34. Y. Takahara, J. N. Kondo, D. Lu and K. Domen, *Solid State Ionics*, 2002, **151**, 305-311.
35. W.-H. Lin, C. Cheng, C.-C. Hu and H. Teng, *Appl. Phys. Lett.*, 2006, **89**, -.
36. H. Kato, K. Asakura and A. Kudo, *J. Am. Chem. Soc.*, 2003, **125**, 3082-3089.
37. D. Zhao, J. Feng, Q. Huo, N. Melosh, G. H. Fredrickson, B. F. Chmelka and G. D. Stucky, *Science*, 1998, **279**, 548-552; M. Kruk, M. Jaroniec, C. H. Ko and R. Ryoo, *Chem. Mater.*, 2000, **12**, 1961-1968.
38. H. Tüysüz, C. W. Lehmann, H. Bongard, B. Tesche, R. Schmidt and F. Schüth, *J. Am. Chem. Soc.*, 2008, **130**, 11510-11517.
39. D. Zhao, Q. Huo, J. Feng, B. F. Chmelka and G. D. Stucky, *J. Am. Chem. Soc.*, 1998, **120**, 6024-6036.
40. M. T. Harris, R. R. Brunson and C. H. Byers, *J. Non-Cryst. Solids*, 1990, **121**, 397-403; R. Aelion, A. Loebel and F. Eirich, *J. Am. Chem. Soc.*, 1950, **72**, 5705-5712.

41. C. V. Teixeira, H. Amenitsch, P. Linton, M. Lindén and V. Alfredsson, *Langmuir*, 2011, **27**, 7121-7131.
42. J. N. Israelachvili, D. J. Mitchell and B. W. Ninham, *Journal of the Chemical Society, Faraday Transactions 2: Molecular and Chemical Physics*, 1976, **72**, 1525-1568.
43. T. Grewe, X. Deng and H. Tüysüz, *Chem. - Eur. J.*, 2014, **20**, 7692-7697.
44. R. V. Goncalves, R. Wojcieszak, P. M. Uberman, S. R. Teixeira and L. M. Rossi, *Phys. Chem. Chem. Phys.*, 2014, **16**, 5755-5762; C. T. S. Hashimoto, A. Murata, T. Sakurada, *J. Surf. Anal.*, 2006, **13**, 14-18.
45. V. Shanker, S. L. Samal, G. K. Pradhan, C. Narayana and A. K. Ganguli, *Solid State Sci.*, 2009, **11**, 562-569.
46. N. G. Teixeira, A. Dias and R. L. Moreira, *J. Eur. Ceram. Soc.*, 2007, **27**, 3683-3686.
47. T. Tsuchiya, H. Imai, S. Miyoshi, P.-A. Glans, J. Guo and S. Yamaguchi, *Phys. Chem. Chem. Phys.*, 2011, **13**, 17013-17018.
48. C. Joseph, P. Bourson and M. D. Fontana, *J. Raman Spectrosc.*, 2012, **43**, 1146-1150.
49. L. An and H. Onishi, *ACS Catal.*, 2015, **5**, 3196-3206.
50. W.-H. Lin, C. Cheng, C.-C. Hu and H. Teng, *Appl. Phys. Lett.*, 2006, **89**, 211904.
51. R. N. T. W. H. Knausenberger, *J. Electrochem. Soc.*, 1973, **120**, 927-931.
52. D. Jing and L. Guo, *J. Phys. Chem. Solids*, 2007, **68**, 2363-2369.
53. J. Zhao, M. A. Holmes and F. E. Osterloh, *ACS Nano*, 2013, **7**, 4316-4325.
54. T. Sreethawong, S. Ngamsinlapasathian, Y. Suzuki and S. Yoshikawa, *J. Mol. Catal. A: Chem.*, 2005, **235**, 1-11.
55. Y. Noda, B. Lee, K. Domen and J. N. Kondo, *Chem. Mater.*, 2008, **20**, 5361-5367.
56. T. Sreethawong, S. Ngamsinlapasathian and S. Yoshikawa, *J. Mol. Catal. A: Chem.*, 2013, **374–375**, 94-101.
57. Q. Liu, L. Zhang and P. A. Crozier, *Appl. Catal. B: Environ.*, 2015, **172–173**, 58-64.

Table of Contents Entry

Alkali metals incorporated ordered mesoporous tantalum oxide with enhanced photocatalytic activity for water splitting

Tobias Grewe, and Harun Tüysüz*

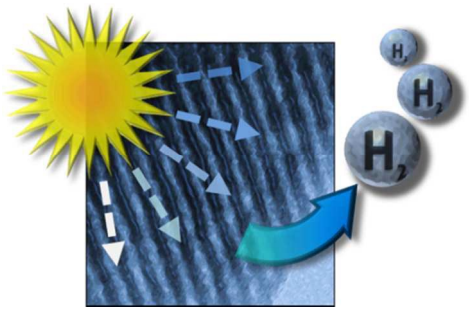

We present a soft-templating synthesis of amorphous ordered mesoporous tantalates with incorporated alkali earth metals for photocatalytic water splitting.